Supplemental Information

Oncogenic RET Kinase Domain Mutations Perturb the Autophosphorylation Trajectory by Enhancing Substrate Presentation In *trans*

Iván Plaza-Menacho, Karin Barnouin, Kerry Goodman, Rubén J. Martínez-Torres, Annabel Borg, Judith Murray-Rust, Stephane Mouilleron, Phillip Knowles, and Neil Q. McDonald
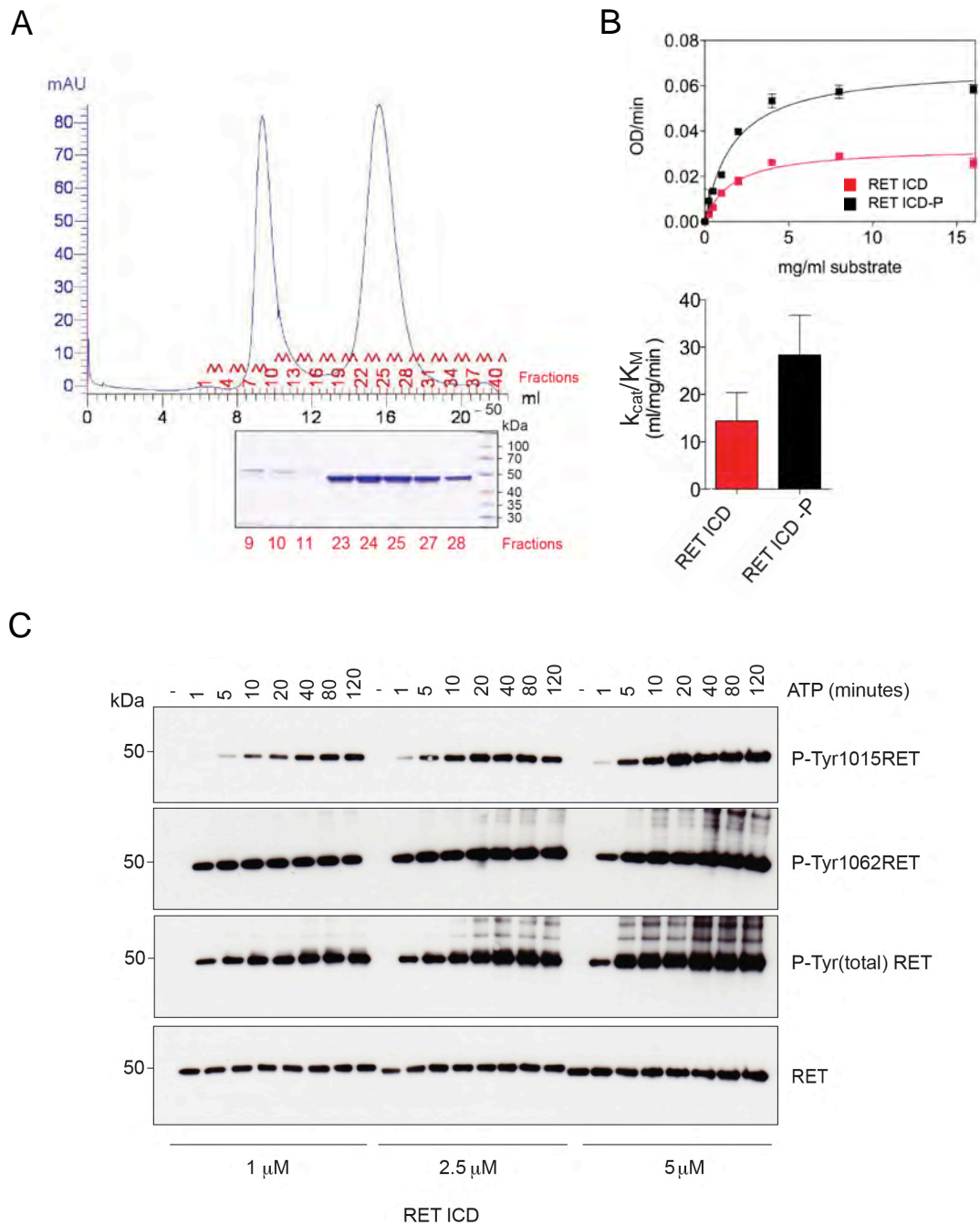
A

B

C

RET ICD

Figure S1 related to Figure 1. RET intracellular domain (ICD) monomeric status, kinase activity and concentration-dependent intermolecular autophosphorylation (autoP).

(A) Size exclusion chromatography (Superdex 200 minicolumn) of RET ICD using a high salt buffer (20 mM Tris pH 7.65, 400 mM NaCl2, 1 mM DTT). Coomassie staining of the indicated fractions (boiled samples) after Western blot (WB) analyses

(inset). (B) Enzyme kinetic analysis of non-phosphorylated versus phosphorylated RET ICD using increasing concentrations of poly-E_4Y peptide. Catalytic efficiency constant k_{cat}/K_M (ml/mg/min) of data represented in B, lower panel. (C) WB analyses of recombinant purified RET ICD at the indicated protein concentrations treated with ATP (5 mM) and $MgCl_2$ (10 mM) for 0-120 min using the indicated phospho-specific RET and total phospho-tyrosine (4G10) antibodies.

A

```
Y1062  TWIENKLYGMSDPNW
Y687   AQAFPVSYSSSGARR
Y905   DVYEEDSYVKRSQGR
Y900   FGLSRDVYEEDSYVK
Y1015  MMVKRRDYLDLAAST
Y1029  TPSDSLIYDDGLSEE
```

B

RET ICD autophosphorylation sites

C

Substrate for RET KDc

D

- Y905 ICD-0P
- Y905 ICD-P
- Y1029 ICD-0P
- Y1029 ICD-P
- Y1062 ICD-0P
- Y1062 ICD-P
- Y687 ICD-0P
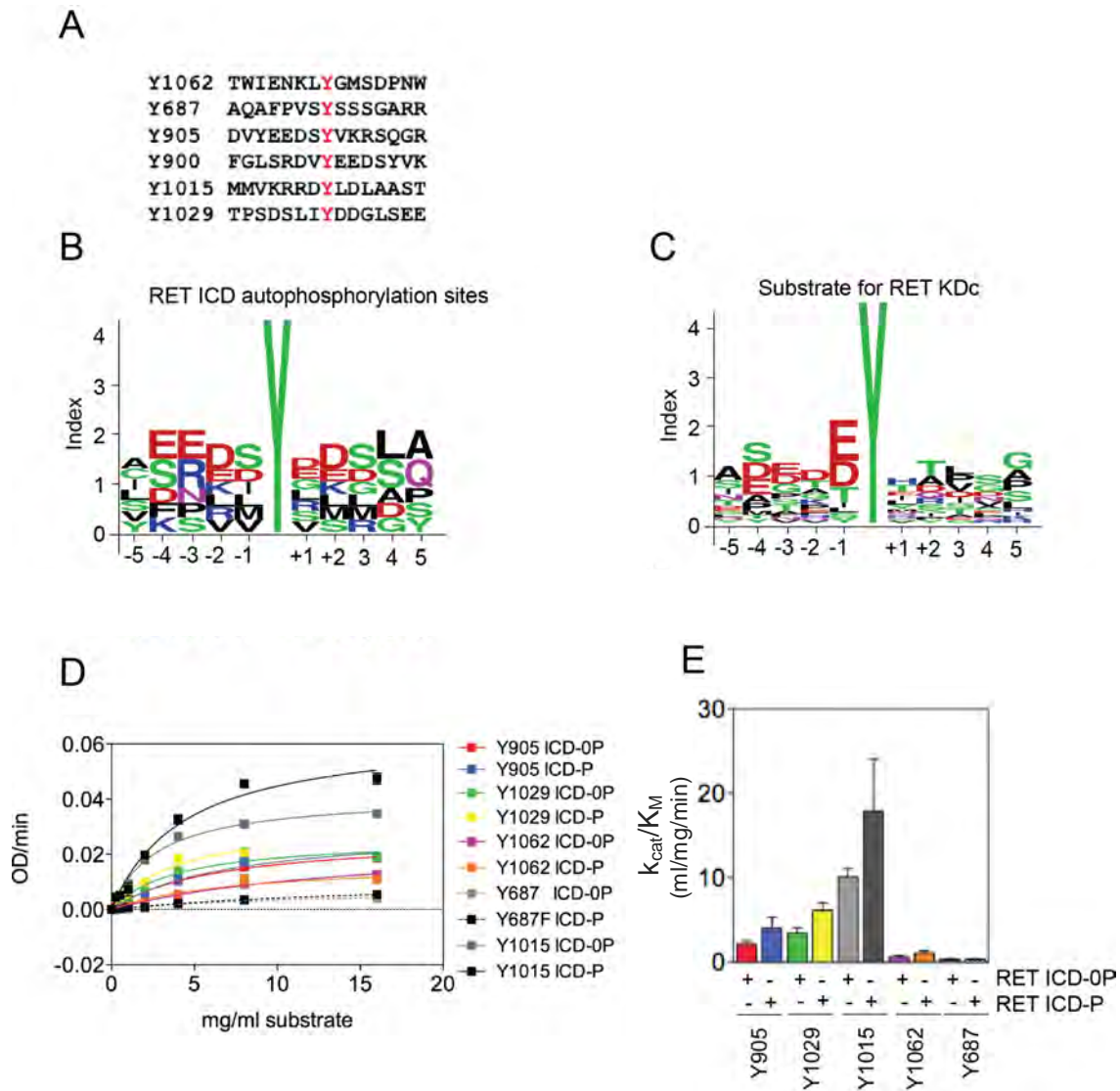- Y687F ICD-P
- Y1015 ICD-0P
- Y1015 ICD-P

E

Figure S2 related to Figure 2. Primary sequence flanking the phosphoacceptor tyrosine sites does not dictate the temporal sequence of RET autoP.

To test if the temporal sequence of RET kinase autoP was determined by the primary sequence surrounding the different phosphorylation sites, we compared the consensus sequence of RET autoP sites obtained by label-free quantitative mass spectrometry (LFQMS, panel A, B) to the consensus sequence of the optimal RET kinase domain (KD) substrate (panel C) previously identified by peptide arrays (Plaza-Menacho et al., 2011). This study showed that wild-type (WT) RET KD core preferentially phosphorylates substrates with acidic residues at the position -1

relative to the Y site, together with a combination of acidic and phosphoacceptor residues S and T at positions -2 and -4. This is consistent with a basic RET core KD with a theoretical pI of 8.9. In general, RTKs prefer peptide substrates with a run of acidic residues at positions N-terminal to the tyrosine phosphorylation site and large hydrophobic residues at the Y + 1 and Y + 3 positions (Songyang et al., 1995). This is also the case for the RET kinase core in principle, but we do not observe a clear preference for large hydrophobic residues at positions +1 and +3. RET autoP sites (Y1062, Y687, Y900, Y905, Y1015, Y1029) show a slight preference for acidic residues E and D at positions -4, -3, -2, however the remaining sequences flanking the phosphorylated tyrosine sites are quite divergent from each other and from an the optimal RET KD core substrate suggesting that primary structure alone does not account for the sequence of autoP. To prove this further, enzymatic assays were performed with the RET ICD in both phosphorylated and non-phosphorylated states against peptides derived from the different phosphorylation sites and the catalytic efficiencies (k_{cat}/K_M) were determined (panel D, E). We observed that: i) enzyme kinetic constants did not follow the same trend observed when RET autoP sites were assessed by LFQMS or WB analysis and ii) phosphorylation status of RET ICD did not change significantly the kinetic constants despite greatly impacting on RET autoP. These data demonstrate that linear peptides as substrates are poor surrogates and have limited utility to assess determinants of RET kinase autoP.
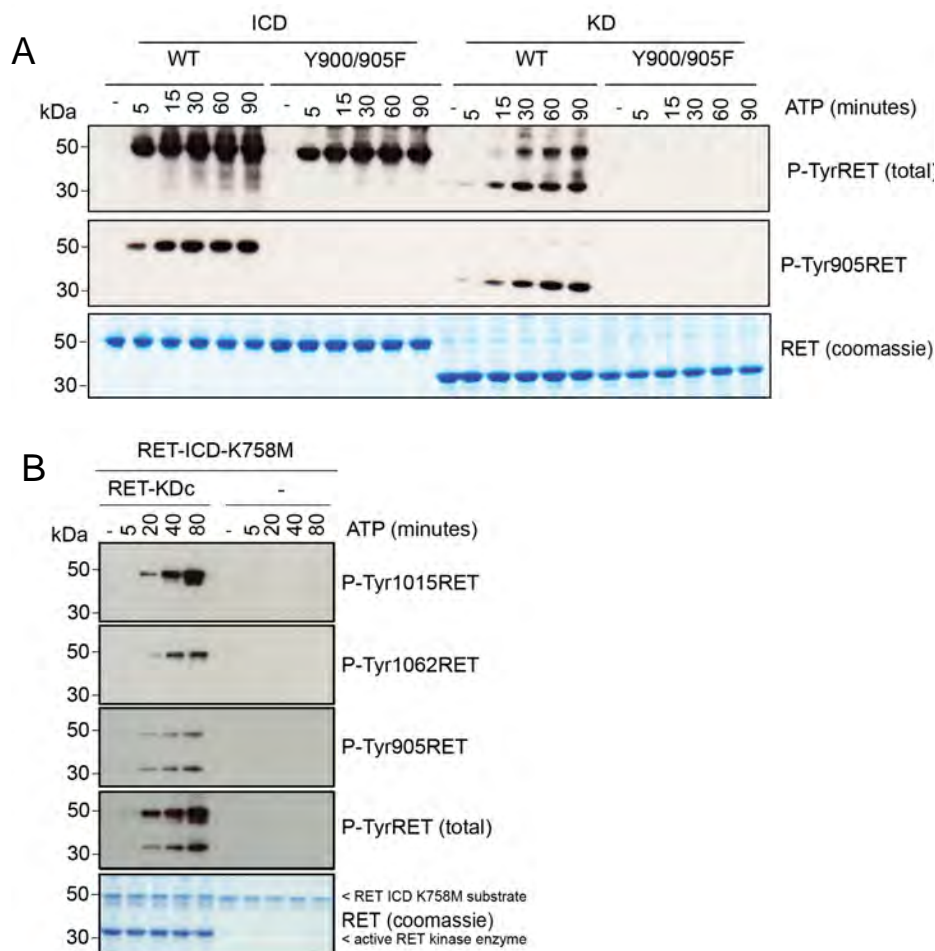
Figure S3 related to Figure 3. Effect of double activation loop (AL) Y/F mutant and RET ICD K758M autoP rescue experiment *in trans* by an active RET KD.

(A) WB analysis of autoP assays comparing WT RET ICD and KD core with double AL Y900/905F mutants stimulated with ATP (5 mM) and $MgCl_2$ (10 mM) for 0-90 min. using the indicated antibodies. Total levels of RET were monitored by Coomassie staining. Equivalent results were obtained in two independent experiments using different protein preparations. (B) Catalytically impaired RET ICD K758M can be rescued *in trans* by an active RET KD core. The catalytic impaired K758M mutant could not undergo autoP upon ATP stimulation by itself. However when used as a substrate, it could be efficiently phosphorylated by an active RET KD core.

Figure S4   Plaza-Menacho et al.
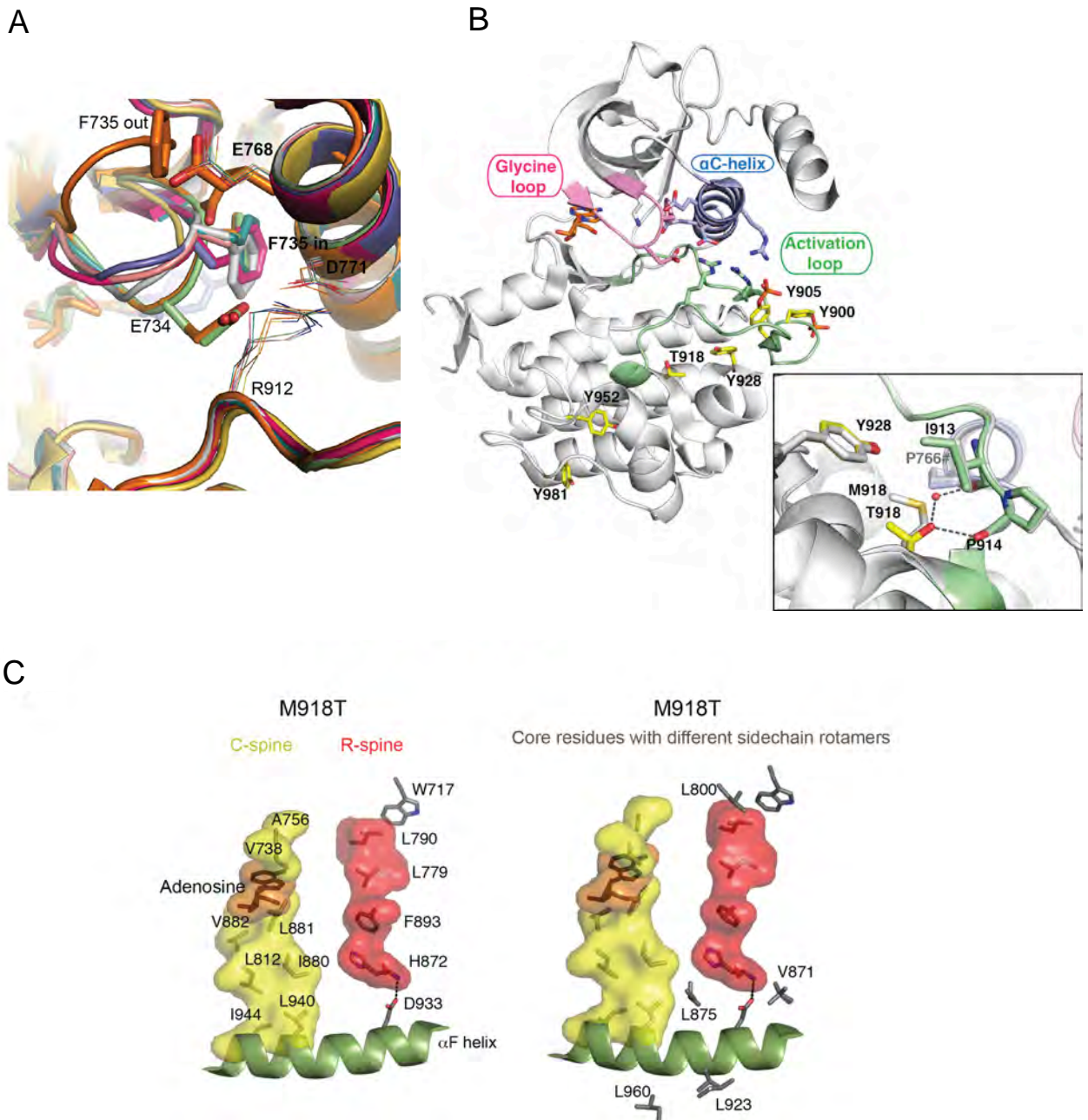
A

B

C

Figure S4 related to Figure 4 and 5. Structural analysis of RET KD crystal structures presented in this study.

(A) Distinct glycine-rich loop (GRL) conformations observed in RET KD crystal structures. Close up of the 'open' and 'closed' GRL conformations from an alignment of all published RET KD crystals structures along with the two presented in this study. Protein structures are shown as cartoons and highlighted residues described in the text defining the two distinct conformers are shown in sticks or lines for clarity:

phosphorylated (p) RET-KD:Ade (PDB ID: 4CKJ), orange; pRETM918T-KD:Ade (4CKI), green; pRET-KD:AMP (2IVT), grey; pRET-KD:PP1 (2IVV), pink; pRET-KD:ZD6474 (2IVU), purple; pRET-KD:X2K (2X2K), dark green; pRET-KD:X2L (2X2L), dark pink; pRET-KD:X2M (2X2M), pale yellow. Ligands are shown as sticks to define the nucleotide pocket. (B) The oncogenic RET M918T kinase structure displayed several features not shared by previously solved structures of the native kinase. It has a double phosphorylated AL on Y900 and Y905, compared to the monophosphorylated (Y905) observed in RET WT KD crystal structures (2IVV, 2 IVT and 2IVU). Furthermore, T918 side chain forms hydrogen bonds with a water molecule and main chain carbonyl from I913 and P914, inset. (C) View of the catalytic (C-) and regulatory (R-) spines of RET M918T (MEN2B) as per text (see below), the right panel shows in addition, side chains of hydrophobic core residues with different rotamers to RET WT. We hypothesize that these differences affect the C-spine and ultimately would indirectly contribute to alter ATP affinity. Further analysis of the two crystal structures presented in this study revealed their close similarity with an overall rmsd of 0.36Å over 290 αC atoms. A closer inspection reveals changes in side chain rotamers for three hydrophobic residues within the RET C-lobe, namely V871, L875 and L923. Both V871 and L875 flank D933 from the αF helix beneath H872 of the regulatory spine. It is unclear from this analysis how to account for the difference in ATP affinity exhibited by the M918T mutant. L923 lies in close proximity to M918 and its side chain rotates towards T918 to partially fill the cavity created by the mutation. We also noticed the adjacent L960 also "flips" its side chain in the M918T structure, in addition to the side chain of L800 within the N-lobe also switches rotamers drawing F709 further into the αC patch, above the αC helix. Recent work has described kinase activation in terms of the linear alignment of the C- and R-spines (Kornev et al., 2008). The larger C-spine of RET contains residues emanating from the hydrophobic αF helix, through to nucleotide and capping N-lobe residues (i.e. L940, I944, L812, I880, L881, V882, V738 and A756). The smaller R-

spine comprises four residues originating from the αF helix. In RET these residues include H872 (from the catalytic HRD motif), F893 (from the DFG motif defining the start of the activation loop), L779 and L790 (an oncogenic site, i.e. L790F). W717 caps this tetrad and is analogous to W342 found in BRAF required for activation and BRAF dimerization (Hu et al., 2013). We previously showed that non-phosphorylated RET core kinase domain (PDB code 2IVT) and the phosphorylated form (PDB code 2IVS) have similar structures and activities in solution towards a poly-E_4Y peptide substrate (Knowles et al., 2006). In agreement with this, we observe that the R-spine is already assembled in a linear alignment consistent with an active kinase both in solution and in the crystals.

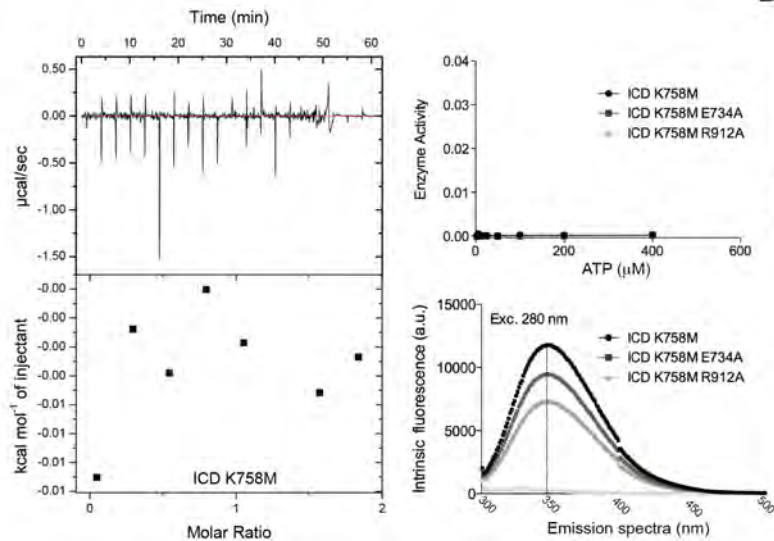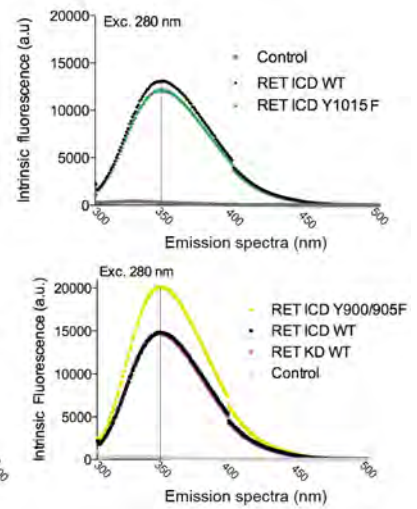**Figure S5   Plaza-Menacho et al.**
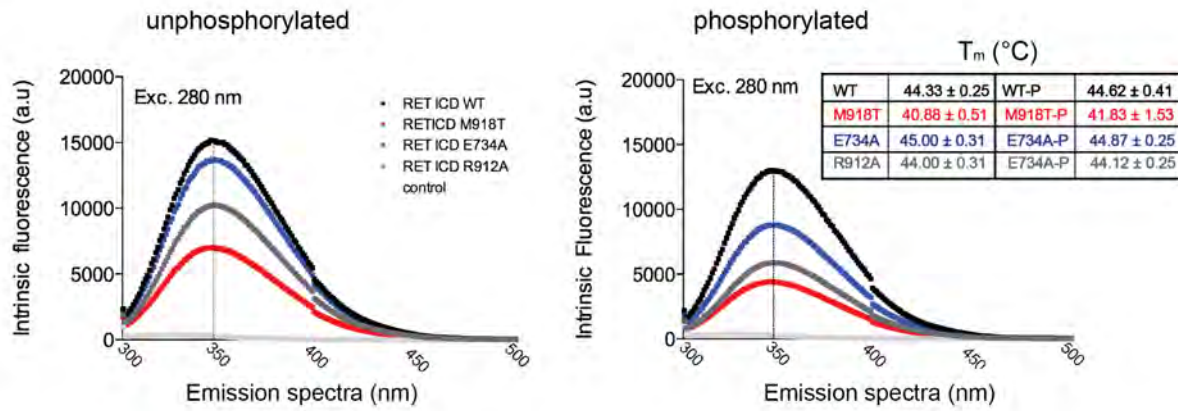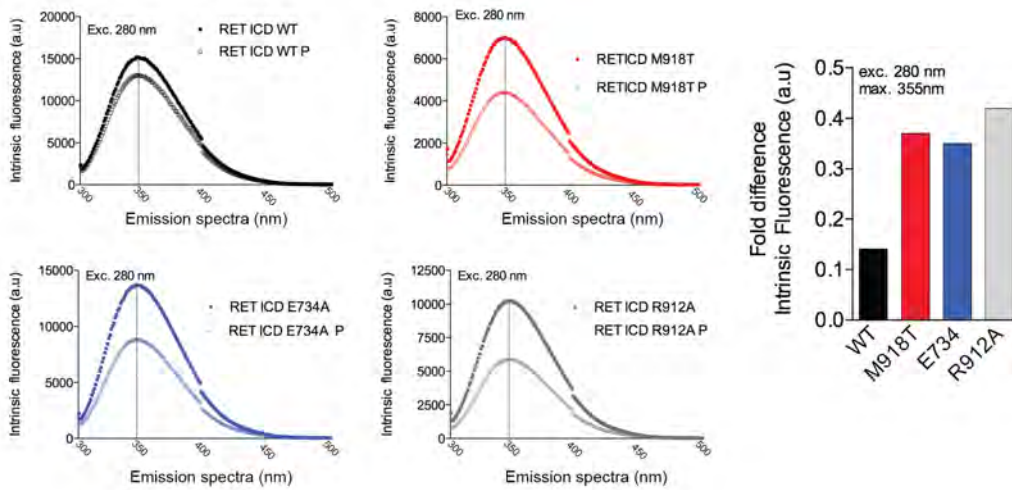
Figure S5 related to Figure 5 and 6. Biophysical characterization of RET ICD (WT and indicated mutants). (A, and inset) Intrinsic fluorescence (IF) and melting temperatures (T_m) for RET ICD WT, oncogenic M918T and (GRL) mutants E734A and R912A in both, non-phosphorylated and phosphorylated forms. IF (arbitrary units, a.u.), emission spectra (307-500 nm) at an excitation wavelength of 280 nm (tryptophan) of indicated recombinant protein (25 µg). Melting temperatures Tm (°C) of A, inset. (B) Comparison of emission spectra profile of RET ICD (WT and indicated mutants) in the non-phosphorylated and phosphorylated forms. RET WT showed small differences in IF upon phosphorylation consistent with crystal structures. On the other hand RET ICD mutants exhibited significant changes in IF consistent with increased flexibility by releasing the AL. Fold difference IF (exc. 280 nm, max. 355 nm) between non-phosphorylated and phosphorylated proteins forms from A, right panel. (C) Isothermal Titration Calorimetric (ITC) profile of ATP-binding to the kinase impaired RET ICD K758M at pH 7.65 at 20 °C. A plot of the heat released (kcal) per mol of ATP added, against the molar ratio of ATP to protein is depicted. The data (filled squares) were fitted to a single sequential-binding model and showed no detectable, ATP interaction, left panel. Enzymatic assay performed with purified recombinant RET ICD K758M, K758M/E734A or K758M/R912A (1 µM) incubated with increasing concentrations of the ATP (0-400 µM) using 8 mg/ml ABL kinase-derived peptide (EAYAAPFAKKK). Data shown is the mean ± SE of two experiments, right upper panel. IF (exc. 280 nm and emission spectra 307-500 nm) of recombinant purified (25 µg) RET ICD K758M, K758M/E734A, and K758M/R912A, right lower panel (D) Further controls included comparison of RET ICD WT with Y1015F mutant showing the same IF profile; and a comparison of WT RET ICD and KD, both displaying the same profile, consistent with the AL and not the flanking regions driving the conformational changes monitored by IF. Comparison of RET ICD WT with a double AL Y900/905F mutant showed a higher IF profile for the double mutant indicating a more compact conformer.

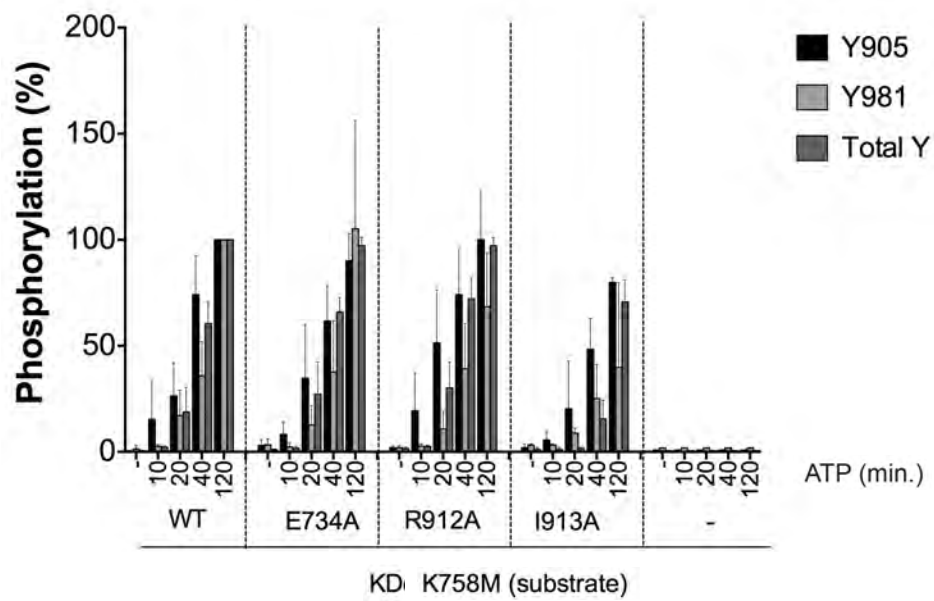**Figure S6   Plaza-Menacho et al.**

A
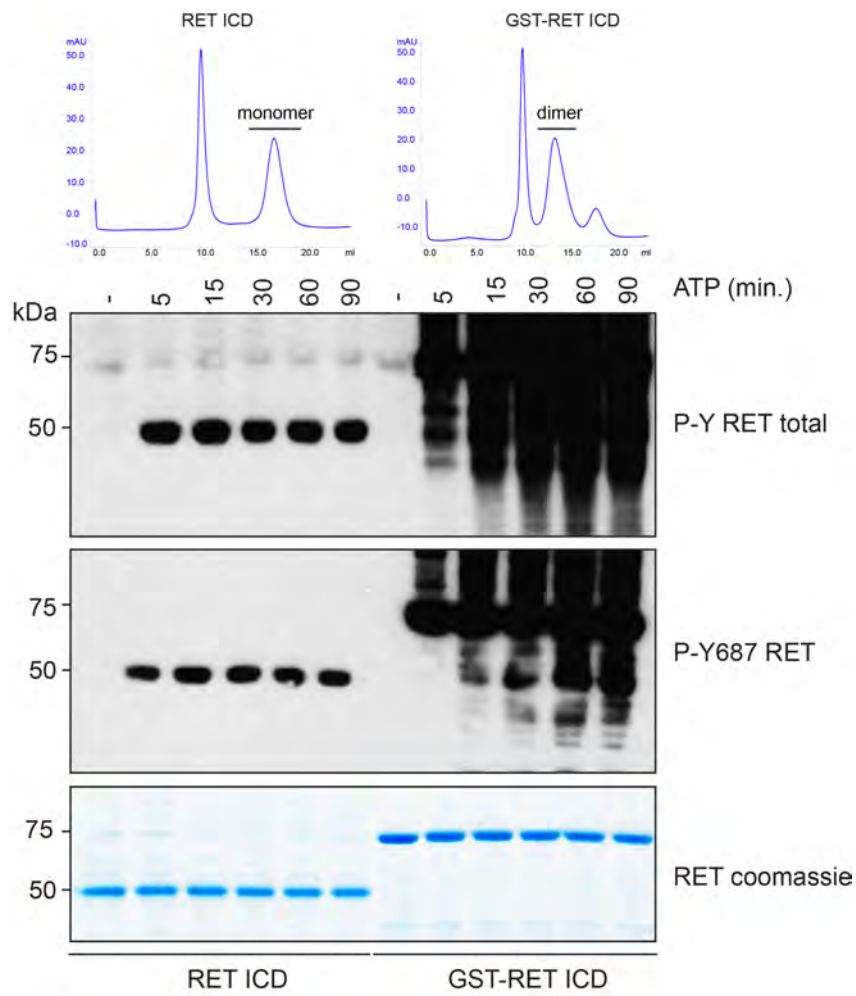
B

Figure S6 related to Figure 6. Dimerization enhances RET kinase autoP and quantification of catalytically impaired RET K758M KD (i.e. substrate) phosphorylation *in trans* by GRL tether mutants.

(A) Size exclusion chromatography (Superdex 200) profiles for RET ICD (monomer) and GST-RET ICD (dimer). WB analysis of a time course autophosphorylation assay (0-90 min) for RET ICD and GST-RET ICD samples, using the indicated antibodies. Coomassie staining of the analyzed samples, total RET. (B) Quantification by densitometry analysis (ImageJ) of catalytically impaired RET K758M KD phosphorylation *in trans* (autoP rescue) by RET ICD WT and GRL tether mutants from 0-120 min. Data represent the mean (percentage of phosphorylation) ± SE of data depicted on Fig. 6A.
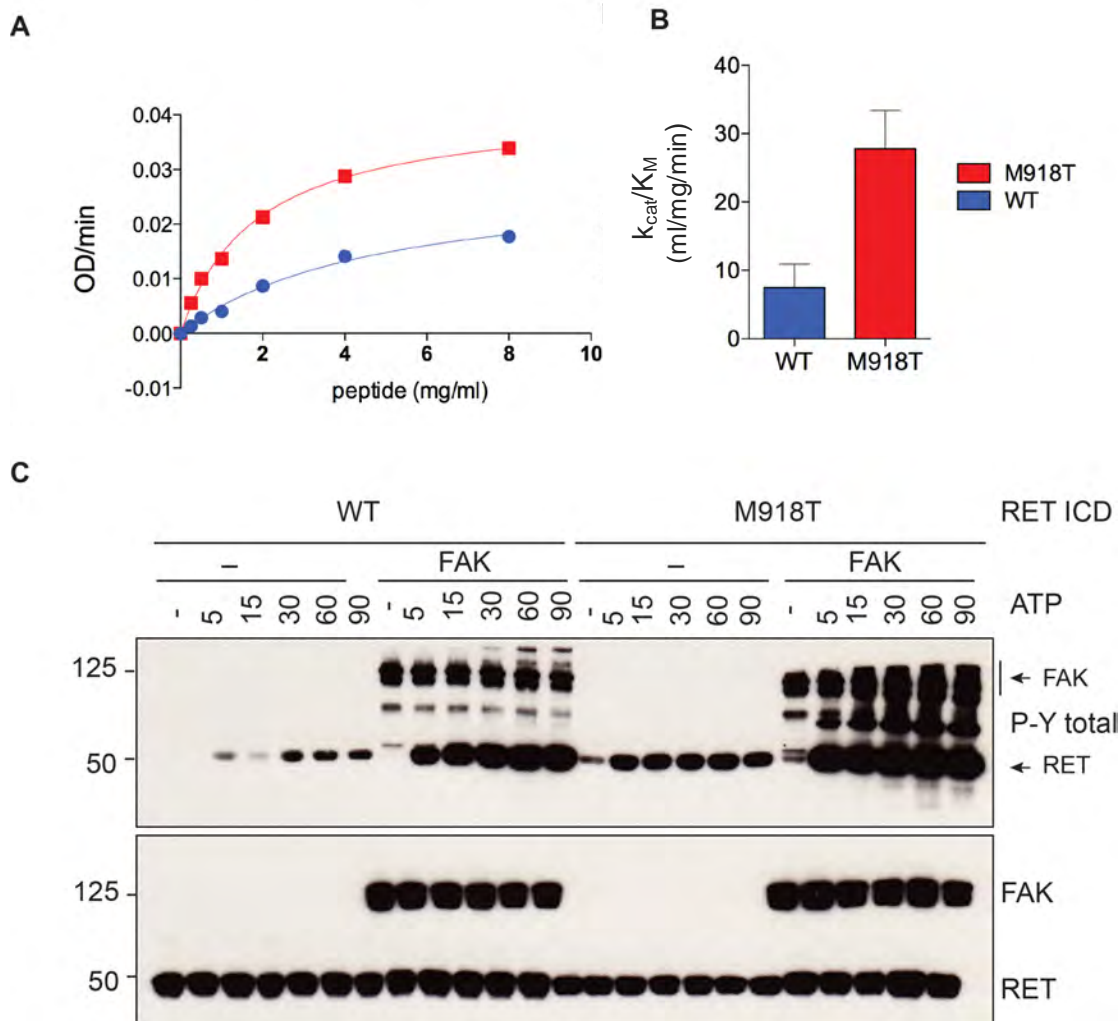
Figure S7 related to Figure 5. Enhanced enzymatic activity of RET M918T measured using an exogenous substrate.

(A) Enzyme kinetic analysis of non-phosphorylated RET ICD WT and oncogenic M918T using increasing concentrations of ABL peptide EAYAAPFAKKK. (B) Catalytic efficiency k_{cat}/K_M (ml/mg/min.) of data from A. (C) WB analysis of recombinant RET ICD WT and M918T incubated in the presence or in the absence of recombinant full length human FAK kinase (GST tagged) with ATP (5 mM) and $MgCl_2$ (10 mM) for 0-90 min using total phospho-tyrosine and total RET and FAK antibodies, respectively.

Table S1

	ATP				
RET	V_{max} (OD/min)	k_{cat} (min^{-1})	K_M (mg/ml)	k_{cat}/K_M (ml/mg/min)	K_d (μM)
WT	0.074±0.003	36.57±1.62	164.1±15.6	0.222	14.3±0.3
E734A	0.063±0.002	31.06±1.23	159.4±14.3	0.195	17.5
R912A	0.065±0.002	32.17±1.44	294.1±24.2	0.109	8.7±0.2
M918T	0.099±0.002	48.92±1.48	106.3±7.9	0.460	1.14±0.9
V804M	0.077±0.003	38.05±1.33	184.8±20	0.205	nd

Table S1 related to Figure 2, 5 and 6. Rate constants and ATP-binding affinity for RET ICD WT and the indicated mutants. Results represent the mean value ± SE from 2-4 independent experiments with multiple replicates (n=6) per experiment from different protein preparations. Rate constants for ATP were measured against an ABL (EAYAAPFAKKK) peptide (8 mg/ml) and apparent K_d values were obtained by isothermal calorimetry under conditions described in material and methods

Supplemental experimental procedures

Expression and purification of recombinant proteins.

Protein expression was carried out using Sf9 insect cells as previously described (Knowles et al., 2006). Human RET ICD (residues 661-1072) and KD core (705-1013) WT and the indicated mutants proteins were purified following a protocol previously described (Knowles et al., 2006). Briefly, Sf9 insect cells (1-2 x10^6 cells/ml) were infected at MOI of 1 with a recombinant baculovirus expressing RET ICD and KD (or the RET mutants where indicated) and harvested 72 hours post-infection. Harvested cells were lysed on ice by sonication in lysis buffer (50 mM Tris-HCl pH 7.65, 400 mM NaCl, 1mM DTT, 10 mM Benzamidine and 0.2 mM AEBSF) and this lysate was then incubated with previously equilibrated Glutathione beads (Amersham) for 90 min at 4 C^o as a single step affinity chromatography purification. Beads were recovered by centrifugation (500 r.p.m., 5 min) and washed five times with elution buffer (20 mM Tris-HCl, 400 mM NaCl and 1mM DTT). Cleavage from glutathione with recombinant 3C-protease was performed overnight rotating at 4 C^o, followed by size exclusion chromatography using a Superdex200 column where indicated.

Mass-spectrometry.

For mass spectrometry, protein samples were separated using pre-cast 4-12% Bis-Tris gels (Invitrogen) and stained using colloidal Coomassie blue (Invitrogen). Protein bands were excised and incubated overnight with destain solution (50 % acetonitrile and 10mM triethylammonium bicarbonate). Bands were washed with destain solution, dehydrated with 100% acetonitrile and vacuum dried, reduced by incubation with 10 mM DTT for 45 min at 50 C^o, alkylated with 50 mM iodoacetamide at room temperature in the dark and then washed three times with destain and dehydrated once more. Proteins were digested at 37 °C overnight using porcine trypsin (Promega, 50 ng/protein band). Proteolysis was stopped by flash freezing before

addition of 5% formic acid and sonication for 15 min to extract peptides. The extraction was repeated once prior to sample dehydration. Proteolysed samples were resuspended in 16 µl 1% formic acid for 20 min prior to analysis by nano-reverse phase LC-MS using a QTOF 6520 mass spectrometer with Chip Cube™ source interface and 1200 series HPLC running MassHunter B.04.00 (Agilent, USA). Samples were loaded onto a chip containing integrated 40 nl enrichment and 150 mm analytical columns and electrospray needle using 3 µl/min 0.1% formic acid. Peptides were eluted at 300 nl/min using a linear gradient from 10-70% elution buffer (80% acetonitrile/ 20% 0.1% formic acid (v/v)) for 10 min. Within 1 min the gradient was increased to 100% elution buffer and 100% buffer was continued for a further 6 min. Each sample was analyzed twice in data-dependent mode. For this acquisition, MS data was recorded in the 290-2500 m/z range at 6 spectra per second. MS/MS data was acquired in the 57-3000 acquisition mass/charge (m/z) range at 4 spectra per second. All data was acquired in profile mode. The data was searched against UniProt (KB15.5j) and an in-house database containing RET sequences concatenated to UniProt (CRUK_Protein 2011_03 + uniprot_sprot_2011_03) using Mascot Daemon version 2.4.0 (Matrix Science, UK). Search parameters used a peptide tolerance of 10 ppm and a fragment tolerance of 0.05 Da. In addition to statistical scoring, the validity of the data was confirmed by manual curation of the data using Scaffold software 2.1 (Proteome Science, USA).

Mass Spectrometric Label-free Quantitation.

For label-free quantitation three to five biological replicates and three technical replicates were analyzed per condition. Data was acquired using the Agilent's LC-Chip Cube™- 6510 QTOF in MS only mode. MS data was recorded with the settings described above in profile mode with the exception of recording 1 spectrum per second. Data was acquired randomly as determined by list randomizer (http://www.random.org/lists/). Files were imported into Progenesis LC-MS version

4.0.4573.30654 (Nonlinear Dynamics, UK) for LC-MS run alignment and MS peak extraction for label-free quantitation after ion peak identification by MASCOT. Peaks of interest were analyzed and validated using quantitation workflow set up in Excel. The RET phosphopeptide normalized abundances from Progenesis LC-MS software were exported to Excel and renormalized against the relative unmodified RET peptides to zero time-point to compensate for loading differences and ensure an accurate representation of relative phosphopeptide abundances. For final quantitation the median $\log_2$ ratio of phosphorylated/unphosphorylated peptides to time 0 min. were determined. The values for related peptides due to enzymatic missed cleavages containing the same phosphorylation sites were averaged. Statistical analyses were performed across biological replicates (n=3 to 5) using graph pad Prism6.

AutoP assays, SDS-Page and Western blotting (WB).

Unless indicated otherwise, time course autoP assays were performed with recombinant purified RET ICD and/or KD core (2.5 µM) in the presence of saturating concentrations of ATP (5 mM) and $MgCl_2$ (10 mM) for the indicated time points. Reactions were stopped by the addition of 4X loading sample buffer (Invitrogen) with 10% β-mercaptoethanol and boiled for 5 min. after which samples were loaded on gel. Samples were run in a NuPAGE Invitrogen 4-12% Bis-Tris precast gels and WB was performed with the indicated antibodies as previously described (Plaza Menacho et al., 2005; Plaza-Menacho et al., 2007a; Plaza-Menacho et al., 2007b). The following antibodies were used: phospho-Tyr1062 RET (Santa Cruz, Palo Alto, CA, USA), phospho-Tyr905 RET and total RET (C31B4, Cell Signaling Technology, New England Biolabs, UK), phospho-Tyr1015 RET (Abcam), phospho-Tyr981 RET (Encinas et al., 2004), phospho-Tyr687 RET (see below) and total phospho-tyrosine antibody (4G10, Millipore).

Phospho-specific RET Y687 antibody generation.

Polyclonal antisera against phosphorylated RET Y687 was generated by immunizing rabbits with a synthetic peptide (AFPVS**pY**SSSGA) KLH-conjugated via glutaraldehyde following a standard protocol used (Pettingill Technology Ltd. UK).

Enzymatic kinase assays.

Enzyme kinetic experiments were performed as previously described (Knowles et al., 2006; Plaza-Menacho et al., 2011). Briefly, rates of phosphorylation by RET kinase were determined using a continuous ADP-coupled kinase assay with the following synthetic peptides derived from known RET autophosphorylation sites: RETY687 AQAFPVSYSSSGA, RETY905 SYVKRSQGRIP, RETY1015 VKRRDYLDLAA, RETY1029 TPSDSLIYDDGLS and RETY1062 TWIENKLYGMSDPNW. Data represents four experiments with multiple replicates (n=6) from at least two independent protein preparations. For the calculation of the kinetics constants of ATP we use 8 mg/ml ABL peptide EAYAAPFAKKK and concentrations of ATP ranging from 0.5 µM to 1 mM.

Isothermal Titration Calorimetry (ITC).

Binding of ATP to the RET ICD (WT and the indicated mutants) was performed in an ITC_{200} Microcalorimeter (GE Healthcare). The sample cell contained 50 µM of purified recombinant RET intracellular domain, and 1 mM of ATP in the injection syringe to achieve a complete binding isotherm. The buffer for both cell and injection samples was 20 mM Tris pH 7.6, 400 mM NaCl, 10 mM $MgCl_2$ and 500 µM TCEP. Injections of 1.5 µl were dispensed with a 5 second addition time and a spacing of 250 seconds, with a total of 15-20 injections. The stirrer speed was set to 1000 r.p.m. All binding experiments were carried out at 20 °C, with fresh protein samples kept at 4 °C before use. Titration curves were fitted using the MicroCal Origin software, assuming a single binding site mode. Data represent the mean ± SE of 2-3 independent experiments from different protein purifications.

Crystallization, diffraction, data collection and processing.

Crystals of phosphorylated RET KD harboring a M918T mutation were grown at 22 °C by vapor diffusion in sitting drops containing 1.5 µl of protein stock solution (3 mg/ml) mixed with 1 µl of reservoir solution (2.0 M sodium formate and 0.1 M sodium citrate (pH 5.5)), the protein stock solution also contained 2.5 mM ATP and 5 mM $MgCl_2$. Crystals were cryoprotected in 50% paratone and flash frozen in liquid nitrogen and X-ray data sets were collected at 100K an in-house MAR image plate detector and a Rigaku MicroMax-007 X-ray goniometer. Data collection and refinement statistics are summarized in Table1. The data set was indexed with MOSFLM and scaled and merged with SCALA (Winn et al., 2011). Molecular replacement was carried out using the atomic coordinates of the phosphorylated RET KD (PDB code: 2IVT) in MOLREP (Vagin and Teplyakov, 2010). After positioning the molecule, RESOLVE (Terwilliger, 2000) was used in prime-and-switch mode to reduce phase bias. The structure was refined using Phenix (Adams et al., 2010) and model building was carried out in COOT (Emsley et al., 2010). Model validation used PROCHECK (Laskowski and Maryanski, 1993) and figures were prepared using the graphic program PYMOL (http:/www.pymol.org).

For the phosphorylated RET KD bound to adenosine structure, crystallization took place in 2.5 µl sitting drops consisting of 1.5:1 (v:v) mixture of 3 mg/ml phosphorylated RET KD with 3 molar excess AMPPNP and well solution containing 0.1 M sodium citrate pH 5.5, and 1.8–2.3 M sodium formate at 20 °C . The crystals took almost 12 months to grow. Cryoprotection was achieved by soaking the crystals for a few min. in 0.1 M sodium citrate pH 5.5, 1.8–2.3 M sodium formate and 25% glycerol. Crystals were flash-frozen in liquid nitrogen and X-ray data sets were collected at 100K at the I-24 beamline of the Diamond Light Source Synchrotron (Oxford, UK). Data collection and refinement statistics are summarized in Table1. The data set was indexed with MOSFLM and scaled and merge with SCALA (Winn et al., 2011). Molecular replacement was carried out in PHASER (McCoy et al.,

2007) using the atomic coordinates of the RET KD bound to PP1 inhibitor (PDB ID: 2IVV). The structure was refined using BUSTER (Blanc et al., 2004) and Phenix (Adams et al., 2010). Model building was carried out in COOT (Emsley et al., 2010) and model validation used PROCHECK (Laskowski and Maryanski, 1993). Both kinases structures have continuous electron density from Gly700 to Arg1012, (including five N-terminal vector-derived residues), with the exception of kinase insert domain residues 823–843, which are disordered. In both structures RET kinase domain forms a head to tail dimer related by a crystallographic 2-fold axis. The dimer overall arrangement is essentially the same as that found in the phosphorylated RET kinase domain (PDB ID: 2IVT).

Intrinsic Fluorescence (IF).

IF analysis was performed following a similar protocol previously described (Chua et al., 2012). Briefly, 25 µg of RET ICD WT and the indicated mutants were analyzed using a Tecan Safire[2] plate reader, with an excitation wavelength of 280 nm and emission spectra from 307 to 500 nm using a Corning black 384 wells assay plate. Data is representative of multiple independent experiments.

Differential Scanning Fluorimetry (DSF).

Thermal denaturation experiments were performed using DSF. Briefly, 5 µg of each protein was added to 90 µl reaction buffer (20 mM Tris-HCl pH 7.65, 400 mM NaCl and 1 mM Dithiothreitol) and 5 µl of Sypro Orange (Invitrogen) fluorescent dye (1:100 in H_2O) was added to a final reaction volume of 100 µl. Each experiment was repeated at least 4-6 times in a 96-well plate in a Bio-Rad iQ5 thermal cycler, with a temperature gradient from 4°C to 100°C at steps of 0.5°C per min. The results are displayed as the differential of the fluorescence in arbitrary units divided by the differential of the temperature, plotted against temperature. The minimum reading of each curve indicates the melting point (T_m) for each protein, representing the inflection point of the fluorescence curve.

Supplemental references

Adams, P.D., Afonine, P.V., Bunkoczi, G., Chen, V.B., Davis, I.W., Echols, N., Headd, J.J., Hung, L.W., Kapral, G.J., Grosse-Kunstleve, R.W.*, et al.* (2010). PHENIX: a comprehensive Python-based system for macromolecular structure solution. Acta crystallographica. Section D, Biological crystallography *66*, 213-221.

Blanc, E., Roversi, P., Vonrhein, C., Flensburg, C., Lea, S.M., and Bricogne, G. (2004). Refinement of severely incomplete structures with maximum likelihood in BUSTER-TNT. Acta crystallographica. Section D, Biological crystallography *60*, 2210-2221.

Chua, E.Y., Vasudevan, D., Davey, G.E., Wu, B., and Davey, C.A. (2012). The mechanics behind DNA sequence-dependent properties of the nucleosome. Nucleic acids research *40*, 6338-6352.

Emsley, P., Lohkamp, B., Scott, W.G., and Cowtan, K. (2010). Features and development of Coot. Acta crystallographica. Section D, Biological crystallography *66*, 486-501.

Encinas, M., Crowder, R.J., Milbrandt, J., and Johnson, E.M., Jr. (2004). Tyrosine 981, a novel ret autophosphorylation site, binds c-Src to mediate neuronal survival. J Biol Chem *279*, 18262-18269.

Hu, J., Stites, E.C., Yu, H., Germino, E.A., Meharena, H.S., Stork, P.J., Kornev, A.P., Taylor, S.S., and Shaw, A.S. (2013). Allosteric activation of functionally asymmetric RAF kinase dimers. Cell *154*, 1036-1046.

Knowles, P.P., Murray-Rust, J., Kjaer, S., Scott, R.P., Hanrahan, S., Santoro, M., Ibanez, C.F., and McDonald, N.Q. (2006). Structure and chemical inhibition of the RET tyrosine kinase domain. J Biol Chem *281*, 33577-33587.

Kornev, A.P., Taylor, S.S., and Ten Eyck, L.F. (2008). A helix scaffold for the assembly of active protein kinases. Proceedings of the National Academy of Sciences of the United States of America *105*, 14377-14382.

Laskowski, R., and Maryanski, M. (1993). Heavy metals in epigeic fauna: trophic-level and physiological hypotheses. Bulletin of environmental contamination and toxicology *50*, 232-240.

McCoy, A.J., Grosse-Kunstleve, R.W., Adams, P.D., Winn, M.D., Storoni, L.C., and Read, R.J. (2007). Phaser crystallographic software. Journal of applied crystallography *40*, 658-674.

Plaza Menacho, I., Koster, R., van der Sloot, A.M., Quax, W.J., Osinga, J., van der Sluis, T., Hollema, H., Burzynski, G.M., Gimm, O., Buys, C.H*., et al.* (2005). RET-familial medullary thyroid carcinoma mutants Y791F and S891A activate a Src/JAK/STAT3 pathway, independent of glial cell line-derived neurotrophic factor. Cancer Res *65*, 1729-1737.

Plaza-Menacho, I., Mologni, L., Sala, E., Gambacorti-Passerini, C., Magee, A.I., Links, T.P., Hofstra, R.M., Barford, D., and Isacke, C.M. (2007a). Sorafenib functions to potently suppress RET tyrosine kinase activity by direct enzymatic inhibition and promoting RET lysosomal degradation independent of proteasomal targeting. J Biol Chem *282*, 29230-29240.

Plaza-Menacho, I., Morandi, A., Mologni, L., Boender, P., Gambacorti-Passerini, C., Magee, A.I., Hofstra, R.M., Knowles, P., McDonald, N.Q., and Isacke, C.M. (2011). Focal adhesion kinase (FAK) binds RET kinase via its FERM domain, priming a direct and reciprocal RET-FAK transactivation mechanism. J Biol Chem *286*, 17292-17302.

Plaza-Menacho, I., van der Sluis, T., Hollema, H., Gimm, O., Buys, C.H., Magee, A.I., Isacke, C.M., Hofstra, R.M., and Eggen, B.J. (2007b). Ras/ERK1/2-mediated STAT3 Ser727 phosphorylation by familial medullary thyroid carcinoma-associated RET mutants induces full activation of STAT3 and is required for c-fos promoter activation, cell mitogenicity, and transformation. J Biol Chem *282*, 6415-6424.

Songyang, Z., Carraway, K.L., 3rd, Eck, M.J., Harrison, S.C., Feldman, R.A., Mohammadi, M., Schlessinger, J., Hubbard, S.R., Smith, D.P., Eng, C*., et al.* (1995).

Catalytic specificity of protein-tyrosine kinases is critical for selective signalling. Nature *373*, 536-539.

Terwilliger, T.C. (2000). Maximum-likelihood density modification. Acta crystallographica. Section D, Biological crystallography *56*, 965-972.

Vagin, A., and Teplyakov, A. (2010). Molecular replacement with MOLREP. Acta crystallographica. Section D, Biological crystallography *66*, 22-25.

Winn, M.D., Ballard, C.C., Cowtan, K.D., Dodson, E.J., Emsley, P., Evans, P.R., Keegan, R.M., Krissinel, E.B., Leslie, A.G., McCoy, A.*, et al.* (2011). Overview of the CCP4 suite and current developments. Acta crystallographica. Section D, Biological crystallography *67*, 235-242.